

Viscosity parameter in dissipative accretion flows with mass outflow around black holes

Shreeram Nagarkoti^{1*} and Sandip K. Chakrabarti^{2,1†}

¹Indian Centre for Space Physics, Chalantika 43, Garia Station Rd., Kolkata, 700084, India

²S. N. Bose National Centre for Basic Sciences, JD-Block, Salt Lake, Kolkata, 700098, India

Accepted XXX. Received YYY; in original form ZZZ

ABSTRACT

Numerical hydrodynamic simulation of inviscid and viscous flows have shown that significant outflows could be produced from the CENtrifugal pressure supported BOundary Layer or CENBOL of an advective disk. However, this barrier is weakened in presence of viscosity, more so, if there are explicit energy dissipations at the boundary layer itself. We study effects of viscosity and energy dissipation theoretically on the outflow rate and show that as the viscosity or energy dissipation (or both) rises, the prospect of formation of outflows is greatly reduced, thereby verifying results obtained through observations and numerical simulations. Indeed, we find that in a dissipative viscous flow, shocks in presence of outflows can be produced only if the Shakura-Sunyaev viscosity parameter α is less than 0.2. This is a direct consequence of modification of the Rankine-Hugoniot relation across the shock in a viscous flow, when the energy dissipation and mass loss in the form of outflows from the post-shock region are included. If we ignore the effects of mass loss altogether, the standing dissipative shocks in viscous flows may occur only if $\alpha < 0.27$. These limits are tighter than the absolute limit of $\alpha = 0.3$ valid for a situation when the shock itself neither dissipates energy nor any outflow is formed. We compute typical viscosity parameters required to understand spectral and temporal properties of several black hole candidates such as GX399-4, MAXI J1659-152 and MAXI J1836-194 and find that required α are indeed well within our prescribed limit.

Key words: accretion, accretion disks – black hole physics – hydrodynamics – shock waves

1 INTRODUCTION

Outflows in most of the astrophysical objects are considered to be associated with accretion phenomena (Livio 1997). Indeed, they are generally thought to be produced from the boundary layers of the central objects, including black holes (Chakrabarti 1996a, hereafter C96a; Chakrabarti 1999; Das & Chakrabarti 1999), paradoxical as it may sound. In a standard Keplerian disk, where the centrifugal force is totally balanced by gravity, no boundary layer could be formed around a black hole. This is not the case when the angular momentum is ‘not-Keplerian’ such as when the flow is transonic which has low and almost constant angular momentum. Here, the outward centrifugal force slows down the infalling matter forming a static or oscillating shock (see, C96a and references therein) or, even a shock free flow with a broad and diffused centrifugal barrier (Chakrabarti

1997). The post-shock region is the so-called CENtrifugal pressure supported BOundary Layer or CENBOL. It has been shown that a large region of the parameter space allows such a shock formation (e.g., Chakrabarti 1996b, and references therein). When the flow has some viscosity, this parameter space starts to shrink (Chakrabarti & Das 2004). Furthermore, when the thermal energy at the base of the jet is dissipated, the drive required to form outflows is also reduced. So, it is pertinent to ask how the outflow rate depends on both the energy dissipation and the viscosity at the base of the flow, i.e., the CENBOL. Even more important is to know the upper limit of viscosity parameter, when all the flow parameters such as the specific energy and angular momentum at the inner edge of the disk are held constant, which will still allow the formation of shocks in presence of these dissipations. There are estimates of α parameter in accretion disks both from observational and numerical simulations. If these estimates are lower as compared to our limits, it would indicate that CENBOL would form and radiation emitted from it is an integral part of the

* E-mail: srnagarkoti@csp.res.in

† E-mail: chakraba@bose.res.in

spectral and timing properties of black holes. It has been shown recently (Nagarkoti & Chakrabarti (2016) [Paper I]; see also, Kumar & Chattopadhyay (2013), with a different viscous stress prescription), that there is an upper limit on the Shakura & Sunyaev (1973) viscosity parameter above which three sonic points and therefore standing shocks are not possible in a viscous accretion flow. These results were predicted by Chakrabarti (1990a) and Chakrabarti (1996a) in the context of isothermal and polytropic flows respectively where it was shown that the topology of solutions change dramatically beyond a critical value of viscosity. In Paper I, the limit is shown to be $\alpha_{sup} \sim 0.3$. In presence of dissipation at the shock and mass outflow, this limit is likely to change. In the present paper, we address this very important issue and show that indeed, shock dissipation tightens the limit to $\alpha_{sup} \sim 0.27$. If, furthermore, outflows are included, then one requires to have $\alpha_{sup} \sim 0.2$ for shock formation. This reduces the available parameter space even further. Nevertheless, as we show below, this limit is not low enough to prohibit formation of the shocks since even the estimated viscosities in flows from observations are much lower than this value. Thus the observational evidences of shocks which decide on the spectral properties of black holes and shock oscillations in explaining quasi-periodic oscillations (QPOs) remain valid even when outflows from dissipative shocks are present.

In the next Section, we present the model equations used for our study. In §3, we present procedures to solve for the transonic flows properties, including the shock locations. In §4, we discuss how the parameter space, spanned by the specific energy at the inner sonic point and the specific angular momentum on the black hole horizon behave in presence of viscosity, energy dissipation and outflow rate. In §5, we show a similar analysis for the data from outbursts of different black hole candidates. Finally, in §6, we draw our conclusions.

2 MODEL EQUATIONS

We begin with the governing equations as presented in C96a by considering a stationary, axisymmetric flow in vertical hydrostatic equilibrium around a Schwarzschild black hole of mass M_{BH} . This is the so-called 1.5 dimensional hybrid model flow (Chakrabarti, 1989; hereafter C89). The space-time geometry around the black hole is described by pseudo-Newtonian potential first introduced by Paczyński & Wiita (1980). Units of distance and speed are chosen to be $r_g = 2GM_{BH}/c^2$ and c , the speed of light respectively. Here, G is the universal constant. The dimensionless hydrodynamic equations which govern the infall of matter are given by (C96a),

i. The radial momentum equation:

$$v \frac{dv}{dx} + \frac{1}{\rho} \frac{dP}{dx} + \frac{l_K^2 - l^2}{x^3} = 0, \quad (1)$$

ii. Continuity Equation:

$$\frac{d(\Sigma xv)}{dx} = 0, \quad (2)$$

iii. Azimuthal Momentum Equation:

$$v \frac{dl}{dx} + \frac{1}{\Sigma x} \frac{d(x^2 W_{x\phi})}{dx} = 0, \quad (3)$$

iv. Entropy Equation:

$$\Sigma v T \frac{ds}{dx} = \frac{hv}{\gamma - 1} \left(\frac{dP}{dx} - \gamma \frac{P}{\rho} \frac{d\rho}{dx} \right) = Q^+ - Q^-. \quad (4)$$

Here, x is the radial distance from the black hole along the disk on the equatorial plane. The local variables v , ρ , P , l_K and l in above equations are the radial velocity, density, isotropic pressure, Keplerian angular momentum and specific angular momentum of the flow respectively. Also, $n = \frac{1}{\gamma - 1}$, γ being the polytropic index: $P \propto \rho^\gamma$. Define Σ and W to be the vertically averaged density and pressure given by $\Sigma = \int_{-h/2}^{h/2} \rho dz = \rho I_n h$ and $W = \int_{-h/2}^{h/2} P dz = P I_{n+1} h$ where $I_n = \frac{(2^n n)!}{(2n+1)!}$ (Matsumoto et al. 1984). $W_{x\phi}$ is the viscous stress tensor given by $W_{r\phi} = -\alpha \Pi$ (C96) which is responsible for the angular momentum transport where $\Pi = W + \Sigma v^2$. Also, s is the entropy density of the flow, T is the local temperature, Q^+ and Q^- are the heat gained and lost by the flow (integrated vertically) respectively. The thickness of the disk, $h(x)$ is given by the relation $h \sim ax^{1/2}(x-1)$ which is obtained by balancing a component of gravitational force and the pressure gradient term in vertical direction, where a is the adiabatic sound speed.

The heating term, Q^+ , is calculated by using mixed stress prescription (C96a). Here, two forms of the viscous shear stresses, $W_{x\phi}(1) = -\alpha \Pi$ and $W_{x\phi}(2) = \eta x \frac{d\Omega}{dx}$ are used, where, η is the dynamic coefficient of viscosity. Heating term is calculated using the formula, $Q^+ = W_{x\phi}^2 / \eta$, where, $W_{x\phi}^2 = W_{x\phi}(1)W_{x\phi}(2)$ and $\Omega = l/x^2$. Cooling term Q^- is set to zero.

3 SONIC POINT ANALYSIS

The sonic point analysis is carried out in the standard way (C89, C90a, C96a; Paper I, and references therein). After some algebra from the governing equations, we obtain:

$$\frac{dv}{dx} = \frac{N}{D}, \quad (5)$$

where,

$$N = N_1 - N_2, \quad D = D_1 + D_2,$$

$$N_1 = \left[\frac{l^2}{x^3} - \frac{1}{2(x-1)^2} + \frac{a^2}{\gamma} \frac{5x-3}{2x(x-1)} \right] \left[\frac{(\gamma+1)a}{\gamma(\gamma-1)} - \frac{2Aw\alpha g a}{\gamma v^2} \right],$$

$$N_2 = \frac{a^3}{\gamma^2} \frac{5x-3}{2x(x-1)} + \frac{a}{\gamma} \left[\frac{2Aw}{vx^2} - \frac{A\alpha w^2}{x\gamma v^2} \right],$$

$$D_1 = v \left[\frac{-(\gamma+1)a}{\gamma(\gamma-1)} - \frac{2Aw\alpha g a}{\gamma v^2} \right] - \frac{a^2}{v\gamma} \left[\frac{-2a}{(\gamma-1)} - \frac{2Aw\alpha g a}{\gamma v^2} \right],$$

$$D_2 = \frac{Aw\alpha a}{v\gamma} \left[1 - \frac{ga^2}{\gamma v^2} \right],$$

$$A = -\alpha I_n / \gamma, \quad g = I_{n+1} / I_n, \quad \text{and} \quad w = ga^2 + \gamma v^2.$$

At the sonic point, both N and D must become zero simultaneously. Equating D to zero, we obtain an expression for the Mach number at the sonic point. Likewise, when we equate N to zero, expression for sound speed at the sonic points can be calculated. With this, all other variables such

as specific angular momentum and energy of the flow can be calculated. Here, inner sonic point x_{in} , specific angular momentum at the horizon, namely, l_{in} , and α are taken as initial parameters to calculate l and E at all radial distances. The angular momentum and specific energy are calculated using the equations (C96a, Paper I)

$$l = l_{in} + \frac{\alpha x a^2 g}{\gamma v} + x \alpha v \quad \text{and} \quad (6a)$$

$$E = \frac{v^2}{2} + n a^2 + \frac{l^2}{2x^2} - \frac{1}{2(x-1)}. \quad (6b)$$

3.1 Procedure to obtain standing shock locations

A flow must have two ‘saddle type’ sonic points to allow a standing shock formation (Chakrabarti 1989; Chakrabarti 1996a; Chakrabarti 1996b, hereafter C96b). The flow originates at the companion surface with negligible radial velocity and gains speed, becoming supersonic after passing through the outer sonic point. It then makes a discontinuous jump to the subsonic branch at a point where shock conditions are fulfilled and passes through the inner sonic point before entering into the black hole supersonically. Several examples of early works are present in C89, C90a and C96a,b. If the conditions are not satisfied, the steady state solution remains smooth, though a weaker barrier is produced.

The shock conditions are modified from the usual Rankine-Hugoniot conditions given in standard text books such as Landau & Lifshitz (1959). To model dissipation from the subsonic post-shock region (CENBOL) which lies between the shock and the inner sonic point, we model energy lost between the pre-shock and the post-shock flow as $\Delta E = n f (a_-^2 - a_+^2)$, as used by Singh & Chakrabarti (2012). Also, the mass outflow rate at shock is written as $\dot{M}_o = \dot{M}_- - \dot{M}_+ = \Delta \dot{M}_+$.

Energy, mass and momentum conservation equations at the shock take the form,

$$E_- - \Delta E = E_+, \quad (7a)$$

$$\dot{M}_- = \dot{M}_+ + \Delta \dot{M}_+ = \dot{M}_+ + \dot{M}_o = (1 + R_{\dot{M}}) \dot{M}_+ \quad \text{and} \quad (7b)$$

$$\Pi_- = \Pi_+ \quad (7c)$$

where, $R_{\dot{M}} = \frac{\dot{M}_o}{\dot{M}_+}$. In the absence of outflows, $R_{\dot{M}} = 0$. Subscripts ‘-’ and ‘+’ represent pre-shock and post-shock quantities at the shock location, x_s .

Starting from x_{in} , we integrate Eq. 5 both inwards and outwards to find the flow topology. The subsonic branch for $x > x_{in}$ will be incomplete and to determine the outer flow boundary conditions, we assume an arbitrary outer sonic point location, say, x_{out} and integrate both inwards and outwards. This flow will also pass through our chosen inner sonic point, only when the shock conditions are satisfied at hereto unknown x_s located somewhere in between x_{in} and x_{out} . We compute shock locations following the above procedure, also described in Paper I. We follow the standard method for calculating the shock conditions (C89, C96a, Mondal et al.

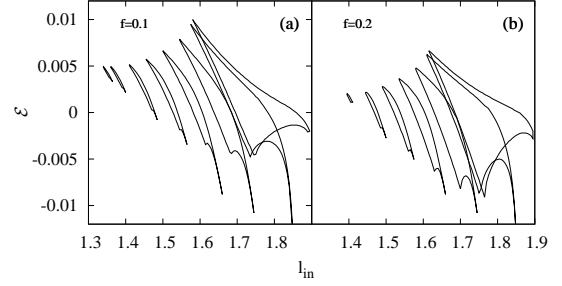


Figure 1. Parameter space which allows dissipative shocks without outflows when (a) $f = 0.1$; $\alpha_{sup} = 0.27$. (b) $f = 0.2$; $\alpha_{sup} = 0.25$.

2014). Because of the dissipation and mass outflow taken into consideration, the Rankine-Hugoniot conditions at the shock must change. The new, modified relation, which connects the Mach numbers in the pre-shock and the post-shock flows is given by,

$$\frac{\left[\gamma M_+^2 + \left(\frac{g}{M_+} \right) \right]^2}{(1 + R_{\dot{M}})^2 \left(n(1 + f) + \frac{M_+^2}{2} \right)} = \frac{\left[\gamma M_-^2 + \left(\frac{g}{M_-} \right) \right]^2}{\left(n(1 + f) + \frac{M_-^2}{2} \right)}. \quad (8)$$

4 PARAMETER SPACE WHICH ALLOWS DISSIPATIVE SHOCKS

4.1 When outflows are absent

First, we assume $R_{\dot{M}} = 0$, i.e., the outflows are absent. For the sake of concreteness, we assume a value of f which represents the fraction of available thermal energy difference between pre-shock and post-shock regions that is dissipated at the shock, presumably due to inverse Comptonization of soft photons. In Eqn. 7a, we assume $f = 0.1$ and 0.2 as examples. Using this method, for each point in the parameter space with specific energy at the inner sonic point \mathcal{E} and the specific angular momentum of flow carried to the horizon, l_{in} , we found the upper limit of α for which shocks are possible namely, α_{sup} . In Fig. 1, we present the parameter space where we plot boundaries of the region in which shocks are present for various values of α . From right to left, the bounded regions are drawn for $\alpha = 0.001, 0.01, 0.05, 0.1, 0.15, 0.2, 0.25$, and 0.27 . The bounded region practically vanishes for $\alpha > 0.27 = \alpha_{sup}$ for $f = 0.1$ and at $\alpha > 0.25 = \alpha_{sup}$ for $f = 0.2$. It is to be noted that for the same set of \mathcal{E} and l_{in} in the parameter space, there could be three sonic points if $\alpha < \alpha_{sh} < \alpha_{cr}$ (Paper I). If $\alpha < \alpha_{cr}$, not only standing shocks are possible, but also oscillating shocks are possible as no Rankine-Hugoniot conditions are fulfilled for $\alpha_{sh} < \alpha < \alpha_{cr}$ (see, analogous situation in Ryu et al. 1997, for inviscid flows). In the present paper, we concentrate only on solutions with standing shock waves.

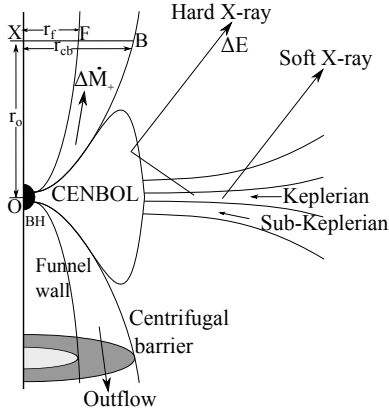


Figure 2. Schematic diagram of the centrifugal barrier and funnel wall in which centrifugal pressure driven winds are found to leave in numerical simulations. Black hole (BH) is at O . OX is the axis of rotation. The radius of funnel wall (r_f) and the radius of centrifugal barrier (r_{cb}) are shown along with the shaded cross-sectional area ($A(r_o)$). Matter lost ($\Delta\dot{M}_+$) at CENBOL pass through this region. Also shown is the energy lost ΔE through inverse Comptonization, for example.

4.2 When outflows are present

In numerical simulations of Molteni et al. (1994) and later in Molteni et al. (1996a), it was shown that outflows are produced from the post-shock region and matter is ejected in between the centrifugal barrier and the funnel wall of thick advective flow. These are later identified as the pressure $P = 0$ and $\nabla P = 0$ surfaces, where P is the gas pressure (C96b).

In Das & Chakrabarti (1999), this outflow region was used to obtain a complete theoretical solution from the accretion to outflow. In Chakrabarti (1999) and Das et al. (2001) outflow rates have been computed and it was found that depending on the strength of the standing shock, a significant amount of matter may be ejected from CENBOL as outflows. It is to be noted that a completely new set of one-dimensional equations governing the energy and mass accretion rate conservation along the z -axis are needed to carry out the outflow properties, since our hybrid model accretion flow (1.5 Dimensional) is not capable of handling the outflow velocity variation.

In recent numerical simulations which include radiative transfer, it was also found that the CENBOL is responsible for the outflows, and the outflow rate starts to decrease with increasing Keplerian disk rate as the CENBOL is cooled down by inverse Comptonization (Garain et al. 2012).

In what follows, we assume that the CENBOL is the origin of the entire outflow. We assume that the outflow has an angular momentum same as that at the launching radius. As discussed above, we assume that the boundaries of the outflow are decided by the $P = 0$ and $\nabla P = 0$ surfaces as were observed in numerical experiments mentioned above. This provides us with an instantaneous cross-sectional area of the flow which is required to compute the velocity profile from which the outflow rate is obtained (Das & Chakrabarti, 1999).

We consider the outflow to be polytropic in nature and the energy and mass conservation equations are written as

(Das & Chakrabarti 1999):

$$E_o = \frac{v_o^2}{2} + na_o^2 + \frac{l_o^2}{2r_m^2(r_o)} - \frac{1}{2(r_o - 1)} \quad \text{and} \quad (9a)$$

$$\dot{M}_o = \rho v_o A_o(r_o), \quad (9b)$$

where the variables pertaining to the outflow contain an ‘o’ as the subscript. Here,

$$r_m(r_o) = \frac{r_{cb}(r_o) + r_f(r_o)}{2} \quad \text{and} \quad (10a)$$

$$A(r_o) = \pi[r_{cb}^2(r_o) - r_f^2(r_o)], \quad (10b)$$

where r_{cb} , r_f and $A(r_o)$ stand for the radius of the centrifugal barrier ($\nabla P = 0$), radius of the funnel wall ($P = 0$) and the area enclosed between these surfaces respectively, see Fig. 2. At the centrifugal barrier, the centrifugal force balances gravity (Molteni et al. 1996a). At the funnel wall, total effective pressure vanishes. So we can write,

$$\frac{l_o^2}{r_{cb}^3} = \frac{r_{cb}}{2r_o(r_o - 1)^2} \quad \text{and} \quad (11a)$$

$$-\frac{1}{2(r_o - 1)} + \frac{l_o^2}{2r_f^2(r_o)} = 0. \quad (11b)$$

As a result, we get the expressions Fig

$$r_{cb}(r_o) = \left[2l_o^2 r_o (r_o - 1)^2 \right]^{1/4} \quad \text{and} \quad (12a)$$

$$r_f(r_o) = l_o (r_o - 1)^{1/2}. \quad (12b)$$

Using equations 9(a-b) we calculate locations of sonic points by standard way as explained earlier. We obtain the equation,

$$\frac{dv_o}{dr_o} = \frac{N_o}{D_o}, \quad (13)$$

where,

$$N_o = \frac{a_o^2}{A^2(r_o)} \frac{dA(r_o)}{dr_o} + \frac{l_o^2}{r_m^3(r_o)} \frac{dr_m}{dr_o} - \frac{1}{2(r_o - 1)^2} \quad \text{and} \quad D_o = v_o - \frac{a_o^2}{v_o}.$$

Following a similar method as earlier, equating D_o with zero, we get the value of Mach no. at the sonic point and equating N_o with zero, we get the value of sound speed at the sonic point. Here, we use $E_o = E_+$ and l_o is the value of angular momentum of the inflow at the shock location.

Subsequently, the ratio, $R_{\dot{M}}$ can be calculated using the formula,

$$R_{\dot{M}} = \frac{\dot{M}_o}{\dot{M}_+} = \frac{a_o^{2n+1} A(r_o)}{2\pi a_+^{2n+1} v_+ x_s^{3/2} (x_s - 1)}. \quad (14)$$

Finally, the ratio of the outflow rate to inflow rate is calculated with the formula,

$$\mathcal{R}_{\dot{M}} = \frac{\dot{M}_o}{\dot{M}_-} = \frac{R_{\dot{M}}}{1 + R_{\dot{M}}} \quad (15)$$

Following the procedure used in the absence of the outflow, we find shock locations as flow parameters are varied. To be concrete, we chose $f = 0.0, 0.1, 0.2$ and 0.3 and obtained the available parameter space having non-zero value

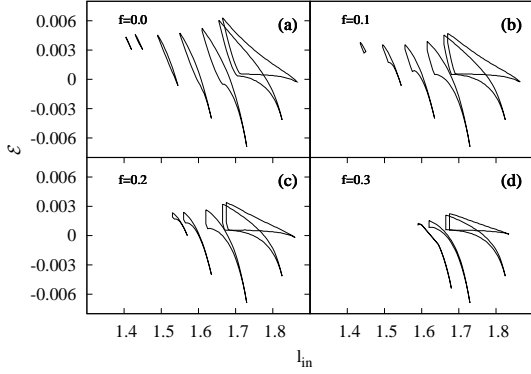


Figure 3. Parameter space allowing dissipative shocks in presence of outflows are shown for (a) $f = 0.0$; $\alpha_{sup} = 0.225$, (b) for $f = 0.1$; $\alpha_{sup} = 0.2$, (c) $f=0.2$; $\alpha_{sup} = 0.125$, (d) $f=0.3$; $\alpha_{sup} = 0.075$.

of $R_{\dot{M}}$ as shown in Fig. 3 (a-d). The highest values of $R_{\dot{M}}$ are 0.13, 0.1, 0.08 and 0.08 when $f=0.0, 0.1, 0.2$ and 0.3 . The curves are drawn for α in the same sequence as those in Fig. 1(a). From right, $\alpha = 0.001, 0.01, 0.05, 0.1, 0.15, 0.2,$ and 0.25 . It is clear that when outflows are included, the parameter space shrinks significantly as can be seen by comparing Fig. 1(a) and Fig. 3(b) when $f = 0.1$ was chosen. In Fig. 3(c), results of $f = 0.2$ are shown. In Fig. 3(d), for $f = 0.3$, the parameter space shrinks even further. When $f = 0.4$, the parameter space of interest is vanished altogether. This shows that when cooling is enhanced, the outflows are choked, supporting the findings of numerical simulations of Garain et al. (2012) that softer states would not have stronger jets (unless there are other effects, such as, magnetic tension which affects the CENBOL dynamically and sporadic and powerful, often superluminal, jets are produced). We also find that the maximum α called α_{sup} for which shocks are possible is monotonically decreasing.

It may be instructive to see how the ratio of outflow rate and inflow rate, namely, $\mathcal{R}_{\dot{M}}$ changes with specific angular momentum in the CENBOL. This is because, in numerical simulations of Molteni et al. (1994) it was pointed out that this outflow is primarily centrifugal force driven. If true, $\mathcal{R}_{\dot{M}}$ generally must have a rising trend with l_{in} . This is also verified from our theoretical work as presented in Fig. 4. As before, the curves are drawn for various α from right to left curve: $\alpha = 0.001, 0.01, 0.025, 0.05, 0.075, 0.1, 0.125, 0.15, 0.175$. It is clear from Fig. 4(a) that the outflow rate decreases gradually as α increases and finally vanishes when $\alpha > 0.175$, when $\mathcal{E} = 0.0027$. Furthermore, rates are higher when the l_{in} is also high. From Fig. 4(b), we observe that only stronger shocks survive when α is increased. Most interestingly, as already shown for inviscid flows in Chakrabarti (1999) and Das et al. (2001), the highest outflow rate is not necessarily seen when the shock is of highest strength. A balance of the CENBOL size and the energy available at the shock plays a major role in deciding this interesting behaviour.

Accordingly, if the base of the jet is more energetic (hot), the outflow rate is expected to be high, even if the

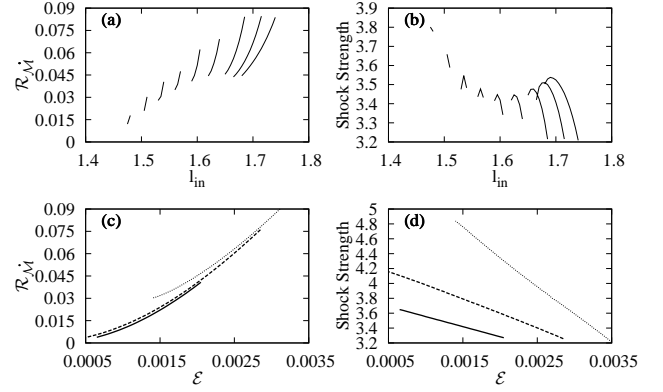


Figure 4. (a) Variation of $\mathcal{R}_{\dot{M}}$ at constant energy, $\mathcal{E} = 0.0027$, $f = 0.1$ for various specific angular momenta with $\alpha = 0.001, 0.01, 0.025, 0.05, 0.075, 0.1, 0.125, 0.125, 0.15, 0.175$. (b) Behavior of shock strength for the same parameters as (a). (c) $\mathcal{R}_{\dot{M}}$ at constant $l_{in} = 1.64$ at $\alpha = 0.05$ for various specific energies with $f = 0.0$ (dotted), 0.1 (dashed) and 0.2 (solid) lines. (d) Behavior of shock strength for the same parameters as in (c).

shock strength is not the highest. In Fig. 4(c-d), we see this behaviour. In Fig. 4(c), we plot $\mathcal{R}_{\dot{M}}$ as a function of \mathcal{E} for various energy dissipation factor f ; $l_{in} = 1.64$ throughout. The more dissipation the shock has, lesser is the outflow rate and the shock strength. These results are very important to link spectral states with outflows. We clearly see that for the spectrally softer states (low temperature of the CENBOL; see Chakrabarti & Titarchuk 1995, hereafter CT95) the outflow rate is lower.

Though the incoming transonic flow and the outflow have positive energies, it is not necessary that the energy of matter entering into the black hole is positive. This is because the matter may dissipate significant amount of energy due to cooling processes (by inverse Comptonization, for example), and eventually the flow becomes bound. The outflow would still be possible with positive energy. This is shown in Fig. 5(a-d) where we demonstrate the general behaviour of the shock strength and $\mathcal{R}_{\dot{M}}$ as functions of specific angular momenta and specific energy. Viscosity parameter $\alpha = 0.05$ was chosen throughout. Each separate curve is for different l_{in} , changing from 1.6 to 1.72 with a step of 0.01 from right to left. For Fig. 5(a and c), there is no dissipation $f = 0$ and for Fig. 5(b and d) the dissipation is significant, $f = 0.2$. In both the cases, the outflow rate generally increases with the specific energy. Lower the energy, higher is the sensitivity. Surprisingly, the strength of the shock does not have this monotonicity. Rather, it reaches the highest value for an intermediate energy.

So far, we have not discussed the actual locations of the CENBOL boundary, i.e., the shock location. Their behaviour is summarized in Fig. 6(a-d). In Fig. 6(a), the energy of the flow is kept fixed at $\mathcal{E} = 0.0027$ and the dissipation is also kept at ten percent level ($f = 0.1$). Variation of shock location (x_s) with different values of l_{in} are drawn for $\alpha = 0.001, 0.01, 0.025, 0.05, 0.075, 0.1, 0.125, 0.15, 0.175$ from the right to the left. In Fig. 6(b), variation of x_s is shown as a function of \mathcal{E} when $l_{in} = 1.64$ and $\alpha = 0.1$ with $f = 0.2$ (solid), 0.1 (dashed) and 0.0 (dotted). The variation

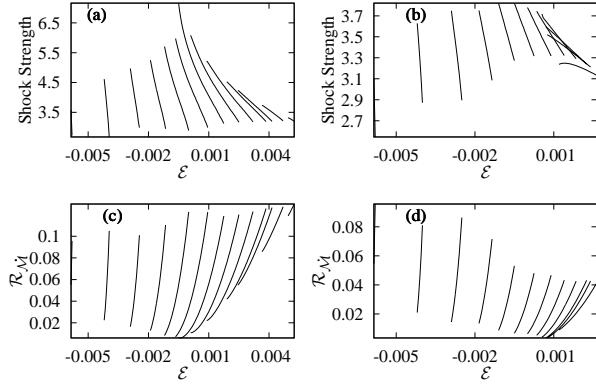


Figure 5. General behaviour of \mathcal{R}_M and shock strength at different cooling in presence of outflow. See text for details.

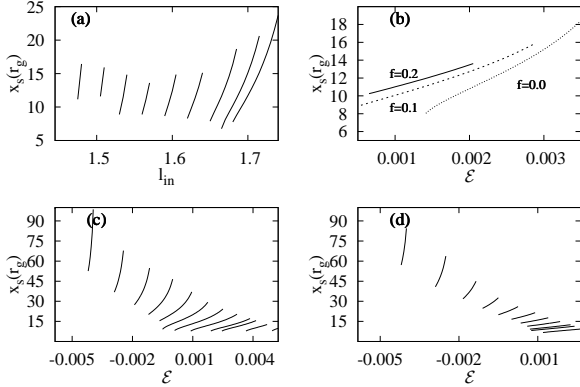


Figure 6. General behaviour of the shock location against (a) l_{in} at constant specific energy, $\mathcal{E} = 0.0027$, $f = 0.1$ and from right to left, $\alpha = 0.001, 0.01, 0.025, 0.05, 0.075, 0.1, 0.125, 0.15, 0.175$, (b) \mathcal{E} at constant $l_{in} = 1.64$, $\alpha = 0.1$ with $f = 0.2$ (solid), 0.1 (dashed) and 0.0 (dotted), and against \mathcal{E} at $\alpha = 0.05$ at $l_{in} = 1.6$ to 1.72 with a step of 0.01 from right to left with (c) $f = 0.0$ and (d) $f = 0.2$.

of x_s is shown with \mathcal{E} for $\alpha = 0.05$, at $l_{in} = 1.6$ to 1.72 with a step of 0.01 from the right to the left in Fig. 6(c) with $f = 0.0$ and in Fig. 6(d) with $f = 0.2$. It is seen that the shock moves outwards with increasing l_{in} and \mathcal{E} . Shock is found to move inwards with increased dissipation.

5 ESTIMATION OF α DURING OUTBURSTS OF VARIOUS SOURCES

In order to check whether theoretical limits on viscosity parameter make sense in real astrophysical systems, we choose a well known outbursting black hole candidate named GX339-4. The general behaviour of the physical parameters have been discussed in Debnath et al. (2015a). They analysed the data of 2010-11 outburst of GX339-4 using two component advective flow model of CT95. From their analysis, the time duration in which the peak of the disk rate followed that of the halo rate was found to be ~ 7 days.

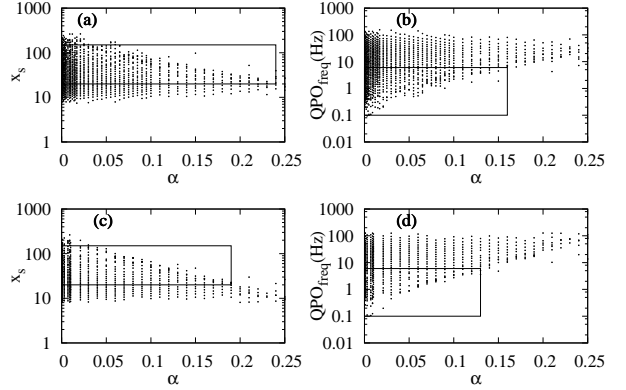


Figure 7. In presence of outflows and in the absence of dissipation at the shock ($f = 0$), (a) all possible x_s , and (b) QPO frequencies are plotted against α . Similarly, when 10% dissipation is considered ($f = 0.1$) in presence of outflows, (c) all possible x_s , and (d) QPO frequencies plotted against α . The rectangles contain values relevant for the 2010-11 outburst of GX339-4.

This we interpret to be the viscous time scale in which the Keplerian matter moves in from the region where X-rays are insignificant in RXTE energy band. The shock location x_s was found to move from ~ 150 to $\sim 20r_g$ and low frequency QPOs were observed in the range ~ 0.1 to ~ 6 Hz in this period.

In Fig. 7, we draw x_s and QPO frequencies against α in presence of outflows as obtained from the propagatory oscillating shock (POS) model of Chakrabarti and collaborators (Chakrabarti et al. 2005, 2008; Debnath et al. 2010, 2013; Nandi et al. 2012). We determine the infall time of matter falling to the black hole using $t_{infall} = \int dt = \int \frac{dx}{v}$ where v is the infall speed obtained from the flow solution for the radial advection of dx . The integration is carried out from the shock location to the inner sonic point. We calculate the frequency of QPO (Molteni et al. 1996b) as $\nu_{QPO} = \frac{1}{t_{QPO}} \approx \frac{1}{t_{infall}}$ in the units of $\frac{r_g}{c}$. QPO frequencies are then converted into the units of Hertz by multiplying the value obtained from the aforementioned formula by the factor $\frac{r_g}{c}$. We use the dynamically obtained mass of GX 339-4, $M_{BH} = 7.5M_{\odot}$ (Chen 2011). This formalism has been used previously by Mondal et al. (2009). Though we use the QPO frequency to be equal to the inverse of infall time, as found in Molteni et al. (1996b), this relation need not be strictly followed (see also Das 2003 and Sukova & Janiuk 2015). Chakrabarti et al. (2015) pointed out that the resonance condition could be satisfied over a wide band of parameter range. Thus our computed α would also have a width as determined below.

Figures 7(a) and (b) are drawn when no thermal dissipation ($f = 0$) is taking place at shock location. Figures 7(c) and (d) are drawn when 10% dissipation is considered ($f = 0.1$). In each Figure, the rectangles contain the region relevant for 2010-11 outburst of GX339-4. The theoretical parameter space allowing the observed values of QPO frequencies and shock locations in the rectangles indicate that allowed α could be as high as 0.13 from the timing properties. Similar analysis of two other outburst sources, namely, MAXI J1659-152 and MAXI J1836-194 have been

done. Based on the constraints imposed by the spectral and temporal data analysis, we find the highest allowed α to be 0.1 and 0.11 respectively. These limits of α are relevant for the advective component of the accretion disk. The uncertainty in α after relaxing the resonance condition would be $\delta\alpha_{sup} \approx \pm 0.015$, which is insignificant.

5.1 Analysis using viscous timescale

In a two component advection flow (TCAF), the viscous Keplerian disk is surrounded by a weakly viscous advective component. These two components have two different rates (CT95) which are obtained by fitting the satellite data with TCAF solution (Debnath et al. 2015a,b; Molla et al. 2016; Jana et al. 2016; Chatterjee et al. 2016). There are ample observational evidences of these two components as well (Smith et al. 2002). These components reach close to the black hole in two different time scales and fitting of outbursting sources indicate that the halo component peaks much before the Keplerian component (Debnath et al. 2015a,b; Molla et al. 2016; Jana et al. 2016; Chatterjee et al. 2016). Difference of these two peak times, assuming that both started at the same time near the outer edge would be due to the fact that the Keplerian component is delayed due to viscosity. Viscous time is the infall time of the viscous, Keplerian disc component from the outer edge to the inner edge of accretion disk. This time can be broken down into the sum of the infall time of disk component from outer edge of disk to the shock location and the infall time of matter from shock location to the inner edge of the disk. The infall time of the latter component is too small (\sim seconds in our case) in comparison to the viscous time (\sim days). If $\alpha_K \gg \alpha_h$, where the subscripts K and h are for the Keplerian disc and sub-Keplerian halo components, the ratio of the two infall time scales would be $1/\alpha_K \gg 1$. Thus the viscous time of the Keplerian component may be safely assumed to be the time duration between the peaks of the halo rate and the Keplerian disc rate.

5.1.1 2010-11 Outburst of GX339-4

In Fig. 3 of Debnath et al. (2015a) it is shown that there is a time delay of ~ 7 days between the peaks of the advective and Keplerian disk components in the 2010-11 outburst of GX339-4. This is interpreted to be due to the viscous time delay of the Keplerian component. In Appendix we show how we calculate the viscous time scale. When we equate our computed time with that of the observed delay, we find that $\alpha_{cr} \sim 0.34$ for GX339-4. Thus, during the rising phase of the outburst, viscosity parameter has evolved from a smaller value in the quiescent state to at least ~ 0.34 when the soft state is reached. During the peak of the soft state, the value of the viscosity parameter could have gone much higher than this. However, turning the source of higher viscosity (e.g., magnetic field entangling inside the disk) off would reduce the matter supply in the Keplerian component and would initiate the declining phase of the outburst. Note that 0.34 is very much higher than 0.13, the highest value to form shocks. Thus the viscosity parameter reaches higher than the critical value in the Keplerian disc component and lower than the critical value in the advective component in order to form shocks.

5.1.2 2010 Outburst of MAXIJ1659-152

If we follow the same procedure to the outburst of MAXIJ1659-152, we find that though its orbital time is only 2.414 hrs, the time duration in which the peak of disk rate followed halo rate was ~ 7 days (Debnath et al. 2015b). In the rising state of the outburst, x_s moves from ~ 360 to $\sim 40r_g$ before the soft intermediate state is achieved. Low frequency QPOs were observed in the range of ~ 1.6 to $6Hz$. Following an analysis similar to the previous case, we find that for MAXIJ1659-152, $\alpha \sim 0.22$ would be enough to cause the formation of the soft state. Here the advective component can have 0.1 as the highest value of the viscosity parameter. Thus the TCAF scenario remains consistent.

5.1.3 2011 Outburst of MAXIJ1836-194

Jana et al. (2016) reported that time duration between the peaks of disk rate and halo rate during 2011 outburst of MAXIJ1836-194 was ~ 10 days. Here, the orbital period is 4.8 hrs. It was observed that x_s changed in the range of ~ 32 to $200r_g$ in the duration of the outburst. Low frequency QPOs were observed in the range ~ 0.4 to $5.2Hz$ during the rising phase of the outburst. Using the same procedure, we find that the Keplerian component could be formed and the soft intermediate state is reached for this source for $\alpha \sim 0.18$. Of course, α could be larger when even softer state is reached. In this case also, the advective component viscosity parameter (0.11) is much lower, which is consistent.

6 DISCUSSION AND CONCLUSIONS

It is intriguing that the matter can indeed resist strong gravitational pull of a black hole if its angular momentum does not redistribute fast enough to create a Keplerian disc. Under this circumstance, matter forms a centrifugal pressure dominated boundary layer from where hot matter may also escape outward driven by the centrifugal force. This feature has been explored by several authors (Das & Chakrabarti 1999; Singh & Chakrabarti 2012; Kumar & Chattopadhyay 2013). With the rise of viscosity parameter, formation of the centrifugal barrier becomes increasingly difficult. One thus requires an answer to the most relevant question in the subject of accretion disc: is viscosity generated inside the disc sufficient to redistribute low angular momentum matter into a Keplerian disc, i.e., maintain a Keplerian distribution in the first place? If not, then one would have a flow with a centrifugal barrier and a shock so that the hot post-shock region (CENBOL) acts as the Compton cloud and produces the observed power-law component as envisaged by CT95. If a Keplerian disk is formed at least on the equatorial region due to viscosity higher than a critical value (CT95) its rate would decide if the CENBOL would remain hot. Most importantly, if CENBOL forms, so does the outflow. Higher rate in the Keplerian component would cool the CENBOL down and produces a spectrally soft state inhibiting the outflow (Chakrabarti & Titarchuk 1995; Chakrabarti 1999; Garain et al. 2012).

In the present paper, using theoretical approach, we answered many questions. We used the appropriate set of equations governing the flow and then modified the

Rankine-Hugoniot condition assuming a viscous dissipative flow having both energy and mass loss. In Paper I, energy loss and outflows from CENBOL were not included. In the present paper we include these after combining the description of the outflow, and formalism of dissipation as present in the literature (Das & Chakrabarti 1999; Singh & Chakrabarti 2012; Kumar & Chattopadhyay 2013). In Kumar & Chattopadhyay (2013) $\frac{d\Omega}{dx}$ was chosen to be continuous which triggers a jump in the angular momentum at the shock, while we use a continuity in angular momentum since we are discussing axisymmetric shocks. This difference induces major changes in the Rankine-Hugoniot conditions, though, some of their conclusions remain similar to those present in our work. In Lanzafame et al. (1998) and Lee et al. (2011) shocks move outward with increasing α as in our present paper where we kept the conditions on the horizon and inner sonic points fixed.

Major conclusions of our work are the followings:

- i) Centrifugal pressure supported standing shocks continue to form even when energy dissipation at the shock and outflows are included.
- ii) The parameter space shrinks more than what was shown in Paper-I in presence of loss of mass and energy at the centrifugal barrier.
- iii) The upper limit of viscosity parameter α_{sup} is reduced to 0.25 and 0.175 respectively when only energy dissipation is included and when both the energy dissipation and outflows are included. This upper limit of α was about 0.3 when neither dissipation and nor outflows are included (Paper I). This implies that the parameter space with standing shocks is reduced.
- iv) The outflow rate increases with lower viscosity and with higher specific angular momentum of the flow. This directly shows that the outflow is centrifugally driven.
- v) The ratio of the outflow rate to inflow rate need not be maximum for the strongest possible shocks, a result which was first presented in Chakrabarti (1999) using a simplified spherical flow geometry.
- vi) As the dissipation at the base of the outflow, namely CENBOL, is increased, the outflow is reduced. This agrees with detailed numerical simulation results of Garain et al. (2012) that spectrally softer states produce lesser outflows.
- vii) Analysis of real data of several black hole candidates show that indeed our theoretical result is very stringent. In real flow, viscosity parameters required when the shocks are found to be formed appear to be well within our limits. Furthermore, we compute viscosity parameters in outbursting sources from the time lag of soft X-rays and found that the required viscosity in the Keplerian component is indeed higher than the critical value. In the advective component, the viscosity is less than the limiting value required for shock formation.

In the literature, there are observations and numerical simulations of magnetized disks which show that the viscosity parameter in a realistic flow cannot be too high. The models relying on magneto-rotational instability (MRI) for the transport of angular momentum (Balbus & Hawley 1991; Hawley & Balbus 1992; Brandenburg et al. 1995; Hawley et al. 1995, 1996) have produced reliable results in simulating magnetized disks. Such numerical simulations show that a value of $\alpha \sim 0.01$ is achieved by such pro-

cess. If values of α greater than this are to be achieved, a net vertical magnetic flux condition has to be imposed (Hawley et al. 1995, 1996; Sano et al. 2004; Pessah et al. 2007). Smak (1999) reported that appropriate value of α in the hot, ionized state during dwarf-novae-outbursts was ~ 0.1 in the Keplerian disk. But taking the measured time intervals between outbursts into account, Cannizzo et al. (1988) suggested the value of α in the cool state to be in the order of ~ 0.01 . Hawley & Krolik (2001) indicated $\alpha \sim 0.1$ in the Keplerian component. It is found that most MRI simulations find the effective value of α to be of the order of 0.01 while the values calculated from observations are of the order 0.1 (King et al. 2007). Since the viscosity of a Keplerian disk has to be above the critical value in order to achieve the distribution within the infall time, such a result is expected.

Combining these results in conjunction with the constraints on viscosity parameter obtained above, we find that centrifugal barriers and shocks are allowed in a realistic flow even with certain amount of energy dissipation (through inverse Comptonization, for instance) and mass loss (outflows). Were the upper limit of α parameter too low, in view of numerical results stated above, the shocks would not have been formed and the advective flow component would have just behaved as a dynamic corona without a strong centrifugal barrier. However, satisfactory fitting of observational data with TCAF (Debnath et al. 2015a,b; Mondal et al. 2014; Jana et al. 2016; Molla et al. 2016; Chatterjee et al. 2016) indicates that the behaviour of CENBOL remained predictable and is indeed an important component of the emission process. Thus the viscosity in the flow cannot be too high (Mondal et al. 2015) to obliterate it, especially in harder states. In presence of magnetic fields threading the CENBOL, the outflow rate would be enhanced removing some angular momentum. Though there is to date no consistent solution which suggests the presence of long range poloidal fields in a turbulent disks we consider, even a small amount of field may affect the dynamics of the flow. So, it would be instructive to study the effects of the fields on the general conclusions we draw here. This will be reported in near future.

ACKNOWLEDGMENTS

Shreeram Nagarkoti acknowledges the support from a fellowship from Abdus Salam International Centre for Theoretical Physics, Italy, which allowed him to pursue the present research.

REFERENCES

- Balbus S. A., Hawley J. F., 1991, ApJ, 376, 214
 Brandenburg A., Nordlund A., Stein R. F., Torkelsson U., 1995, ApJ, 446, 741
 Cannizzo J. K., Shafter A. W., Wheeler J. C., 1988, ApJ, 333, 227
 Chakrabarti S. K., & Titarchuk L. G., 1995, ApJ, 455, 623
 Chakrabarti S. K., 1989a, ApJ, 347, 365 (C89)
 Chakrabarti, S. K., 1990a, Theory of Transonic Astrophysical Flows, World Scientific, Singapore
 Chakrabarti S. K., 1996, ApJ, 464, 664 (C96a)
 Chakrabarti S. K., 1996, MNRAS, 283, 325 (C96b)
 Chakrabarti S. K., 1997, ApJ, 484, 313

Chakrabarti S. K., 1999, *A&A*, 351, 185 (C99)
 Chakrabarti S. K., Titarchuk D., Kazanas L., Ebisawa K., 1996, *AASS*, 120,163
 Chakrabarti S. K., Das S., 2004, *MNRAS*, 349, 649
 Chakrabarti S. K., Molteni D., 1993, *ApJ*, 417, 671
 Chakrabarti S. K., Molteni D., 1995, *MNRAS*, 272, 80
 Chakrabarti S. K., Nandi A., Debnath D., Sarkar R., Datta B. G., 2005, *IJP*, 79, 841 (arXiv:astro-ph/0508024)
 Chakrabarti S. K., Debnath D., Nandi A., Pal P. S., 2008, *A&A*, 489, L41
 Chatterjee D., Debnath D., Chakrabarti S. K., Mondal S., Jana A., 2016, *ApJ*, in press
 Chen T., 2011, *IAUS*, 275, 327
 Das Tapas K., 2003, *ApJ*, 588L, 89
 Das Tapas K., Chakrabarti S. K., 1999, *CQGra*, 16, 3879
 Das S., Chattopadhyay I., Chakrabarti S. K., 2001, *A&A*, 379, 683
 Debnath D., Chakrabarti S. K., Nandi A., *A&A*, 520, 98
 Debnath D., Chakrabarti S. K., Nandi A., 2013, *AsSpR*, 52, 2143
 Debnath D., Mondal S., Chakrabarti S. K., 2015a, *MNRAS*, 447, 1984
 Debnath D., Molla A. A., Chakrabarti S. K., Mondal S., 2015b, *ApJ*, 803, 59
 Frank J., King A., Raine D., 2002, *Accretion Power in Astrophysics*, Third Edition, Cambridge University Press, New York
 Garain S. K., Ghosh H., Chakrabarti S. K., 2012, *ApJ*, 758, 114
 Giri K., Chakrabarti S. K., 2012, *MNRAS*, 421, 666
 Giri K., Chakrabarti S. K., 2013, *MNRAS*, 430, 2836
 Giri K., Garain S. K., Chakrabarti S. K., 2015, *MNRAS*, 448, 3221
 Hawley J. F., Balbus S. A., 1992, *ApJ*, 400, 595
 Hawley J. F., Gammie C. F., Balbus S. A., 1995, *ApJ*, 440, 742
 Hawley J. F., Gammie C. F., Balbus S. A., 1996, *ApJ*, 464, 690
 Hawley J. F., Krolik J. H., 2001, *ApJ*, 548, 348
 Jana A., Debnath D., Chakrabarti S. K., Mondal S., Molla A. A., 2016, *ApJ*, 819, 107
 King A. R., Pringle J. E., Livio M., 2007, *MNRAS*, 376, 1740
 Kumar R., Chattopadhyay I., 2013, *MNRAS*, 430, 386
 Landau L. D., Lifshitz E. M., 1959, *Fluid Mechanics*, Second Edition, Butterworth-Heinemann, Oxford
 Livio M., 1997, *ASPC*, 121, 845
 Lanzafame G., Molteni D., Chakrabarti S. K., 1998, *MNRAS*, 299, 799
 Lee S. J., Ryu D., Chattopadhyay I., 2011, *ApJ*, 728, 142
 Matsumoto R., Kato S., Fukue J., Okazaki A. T., 1984, *PASJ*, 36, 71
 Molla A. A., Debnath D., Chakrabarti S. K., Mondal S., Jana A., 2016, *MNRAS*, in press
 Molteni D., Lanzafame G., Chakrabarti S. K., 1994, *ApJ*, 425, 161 MLC(94)
 Molteni D., Ryu D., Chakrabarti S. K., 1996a, *ApJ*, 470, 460
 Molteni D., Sponholz H., Chakrabarti S. K., 1996b, *ApJ*, 457, 805
 Mondal S., Basu P., Chakrabarti S. K., 2009, *MNRAS*, 396, 1038
 Mondal S., Debnath D., Chakrabarti S. K., 2014, *ApJ*, 786, 4
 Mondal S., Chakrabarti S. K., Debnath D., 2015, *ApJ*, 798, 57
 Nagarkoti S., Chakrabarti S. K., 2016, *ApJ*, 816, 7
 Nandi A., Debnath D., Mandal S., Chakrabarti S. K., 2012, *A&A*, 542, 56
 Paczyński B., Wiita, P. J., 1980, *A&A*, 88, 23
 Pessah M. E., Chan C. K., Psaltis D., 2007, *ApJ*, 668, 51
 Pringle, J. E., 1981, *ARA&A*, 19, 137
 Ryu D., Chakrabarti S. K., Molteni D., 1997, *ApJ*, 474, 378
 Sano T., Inutsuka S., Turner N. J., Stone J. M., 2004, *ApJ*, 605, 321
 Shakura N. I., Sunyaev R. A., 1973, *A&A*, 24, 337 (SS73)
 Singh C. B., Chakrabarti S. K., 2012, *MNRAS*, 421, 1666
 Smak J., 1999, *Acta Astron.*, 49, 391

Smith D. M., Heindl W. A., Swank J. H., 2002, *ApJ*, 569, 362
 Sukova P., Janiuk A., 2015, *MNRAS*, 447, 1565

APPENDIX A: CALCULATING VISCOUS TIMESCALE

The viscous timescale, t_{visc} is given by the relation, $t_{visc} \approx \frac{r^2}{\alpha c_s h} \approx \frac{r^{1/2}(r-1)}{\alpha(\frac{h}{r})^2}$ where, α , c_s , r and h stand for the viscosity parameter, the adiabatic sound speed, radius at outer edge (in units of $r_* = \frac{Gm}{c^2}$), and the scale height of the accretion disk respectively (Pringle 1981). We use the relation $\frac{h}{r} = 2.4 \times 10^{-3} \alpha^{-\frac{1}{10}} \dot{M}^{\frac{3}{20}} m^{-\frac{3}{8}} r_*^{\frac{1}{8}} f^{\frac{3}{8}}$, (Frank et al. 2002) where \dot{M} is accretion rate in the units of $10^{17} \text{erg s}^{-1}$, m is mass of the black hole in units of solar mass, and $f = \left(1 - \frac{1}{r^{\frac{1}{2}}}\right)^{\frac{1}{4}}$. We use $r = 20000$ in general. Using Shakura-Sunyaev disk temperature distribution, $T = 5 \times 10^7 K m^{-\frac{1}{2}} \dot{M}^{\frac{1}{4}} r^{-\frac{3}{4}} f^{\frac{1}{4}}$, we find that the temperature at the outer edge is $\sim 10^4 K$. Here, \dot{M} is the accretion rate of the disk component on the day when advective (halo) component had maximum accretion rate. This paper has been typeset from a $\text{\TeX/L\AA T\AA E X}$ file prepared

by the author.